Dust creation and transport in MAST

G. De Temmerman[1,2], M. Bacharis[3], J. Dowling[2], and S. Lisgo[4]

[1]Present address: FOM Institute for Plasma Physics Rijnhuizen, Edisonbaan 14, 3439 MN Nieuwegein, The Netherlands
[2]EURATOM/CCFE Fusion Association, Culham Science Centre, Abingdon, UK
[3]Blackett Laboratory, Imperial College London, Prince Consort Road, London, SW7 2BZ, UK
[4]ITER Organization, CEA-Cadarache Centre, 13108 Saint Paul les Durance, France

E-mail: g.c.temmerman@rijnhuizen.nl

Abstract.

In this contribution, we report on experiments performed in MAST to investigate dust creation, transport and influence on plasma performance. The exceptional diagnostic access of MAST allows stereoscopic imaging of dust particles motion in both the divertor and the main chamber, utilising fast infrared cameras. This technique allows the 3D trajectory of the particles to be reconstructed. Infrared imaging of dust creation during disruptions revealed an isotropic release of dust particles from the surface with very high velocities (up to 350 m.s^{-1}). Stereoscopic imaging has been used to study, for the first time, the mobilization and transport in the divertor plasmas of carbon and tungsten particles with known size distributions, which were introduced into the vessel through a divertor probe. A correlation between the carbon particle size and acceleration by the plasma is observed. Tungsten particles are found to move with lower velocities and experience lower acceleration and are found to be more prone to vertical motion towards the core plasma. In the case of large particles this can lead to early disruptions. Modelling of the dust injection experiments has been conducted using the DTOKS code in an attempt to validate the transport equations employed in the simulation.

PACS numbers: 52.40.Hf, 52.77.Dq

1. Introduction

The presence of dust particles in fusion devices has been recognized for a long time [1]. Those particles are created both from the intense plasma-material interactions inherent to fusion devices and also during maintenance periods due to in-vessel work and flaking of co-deposits due to oxidation in air. In most modern tokamaks, dust generally does not represent a problem for plasma operations although it has been observed in the past that dust particles could seriously impede the startup phase of a discharge [2]. In addition, it has recently been observed that long discharges in LHD can be terminated early because of the entrance into the core region of a large dust particle coming from the wall [3]. Dust generation by flaking of co-deposits in Tore Supra during a campaign of long pulse operation without intershot cleaning, was found to increase during the campaign. The largest flakes lead to early termination of the discharge [4]. The problems associated with dust particles in fusion devices are thus expected to be significantly enhanced in ITER, due to the large increase in duty cycle and material migration.

The problem is actually multifold, due to additional safety issues. Dust can be radioactive, toxic and explosive when reacting with steam and air. In order to control the potential safety issues, the quantity of dust in ITER must remain below safety limits which comprise mobilizable dust in the vacuum vessel (1 ton) and dust on hot surfaces (6 kg of Be and C dust), the latter being driven by the chemical reactivity of hot dust with steam [5].

Dust particles can be created as a consequence of different plasma-material interaction mechanisms like erosion, arcing, flaking of co-deposited layers and brittle destruction [6, 7, 8]. Dust production is expected to be significant during transient events (ELMs, disruptions) and indeed large numbers of particles are observed with visible cameras in DIII-D during Vertical Displacement Events (VDE) when the plasma makes contact with the top of the vessel [9]. ELM simulation experiments in linear devices have also evidenced significant droplet ejection from tungsten targets which will constitute a significant source of dust particles [10]. Dust particles created during disruptions might settle in regions of the machine where the next plasma discharge can access them, and it is thus of high interest to evaluate the operational risk these particles can represent.

In this contribution, we report on experiments performed in MAST to investigate dust creation, transport and influence on plasma performance. Dust generation during disruption has been studied using a fast infrared camera, allowing the determination of the particle velocities. The exceptional diagnostic access of MAST allows stereoscopic imaging of dust particles motion in both the divertor and the main chamber, utilising fast infrared and visible cameras. This technique allows the 3D trajectory of the particles to be reconstructed. The mobilization and transport of carbon and tungsten particles with known size distributions and compositions, which were introduced into the vessel through a newly installed divertor probe (the Divertor Science Facility), has been studied for the first time under similar plasma conditions.

2. Experimental

2.1. The Divertor Science Facility

A dedicated sample manipulator, the Divertor Science Facility (DSF) has been designed and installed on the MAST tokamak. The design of the system has been inspired by that of the DIMES probe on DIII-D [11]. The system is designed to allow an easy acess to the outer divertor for sample exposure, impurity injection and electrostatic probes. Insulation of the DSF from the main vacuum chamber is done with a UHV valve which allows sample exposure and retrieval without requiring a vessel vent. A pneumatic linear drive is used to insert the DSF head into the divertor floor, and a register pin ensures the correct positioning of the DSF head into the outer divertor tile. The DSF head comes flush with the divertor tiles which in MAST have an imbricated structure with an angle of 4 degrees [12]. Figure 1 shows a general view of the system attached to the MAST vessel and a view of the probe head fully inserted. The plasma exposed surface dimensions are 37x34 mm. The system location was chosen to maximize the number of diagnostics which could observe the DSF head. This includes 2 infrared cameras, 1 filtered visible camera and a survey spectrometer. In addition, arrays of divertor langmuir probes allows the determination of the plasma parameters at the location of the DSF head.

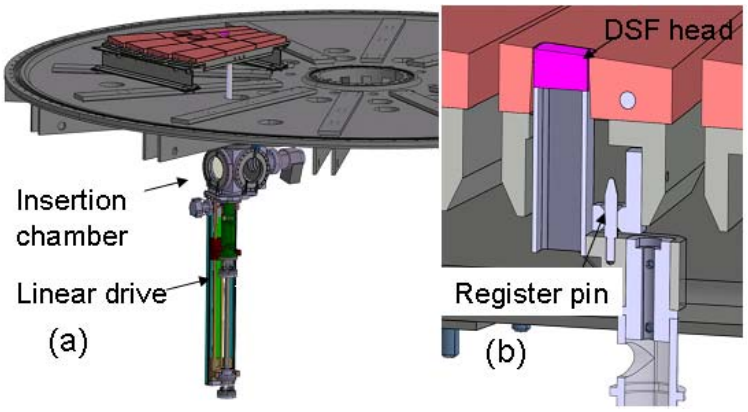

Figure 1. (a) Schematic overview drawing of the Divertor Science Facility showing the insertion system and the independent pumping system. The drawing shows the DSF configuration when the head is fully inserted into the machine, while (b) shows a zoomed view of the DSF head inserted into the MAST graphite divertor tile. The DSF head comes flush with the surface.

A turbopump attached to the system is used to evacuate the insertion chamber. Before insertion, the system is pumped down and baked out to achieve a base pressure of 1-5$\times 10^{-8}$mbar. A feedthrough chamber located at the bottom of the system is equipped with 4 flanges allowing electrical connections as well as gas lines to be connected to the system. It should be mentioned that the system is designed to allow an easy decoupling from the MAST vacuum vessel. A dedicated trolley is designed to maintain the system

while the fixation bolts from the DSF to the main chamber are removed. The whole trolley is then lowered down and the whole DSF assembly can be transported to the laboratory.

2.2. Introduction of dust into the outer divertor

A fine grain graphite head was used as a sample holder for the dust particles, similarly to what was done previously in DIII-D [13]. Nine dimples (2 mm diameter, 1 mm deep) have been made on the head surface (figure 2a). The dimples are filled with dry dust, the dust head is weighed before the experiment to determine how much dust has been put on the head. Once filled, the dust head was installed on the DSF. During transportation between the lab and the torus hall, the head was contained in a plastic bag to avoid dispersion of the powder.

Two types of dust particles were used. The graphite dust, consisting of 0.5-10 μm flakes with a 6 μm median diameter, was similar to that used in [13]. The tungsten dust was supplied by Buffalo Tungsten Inc. and has a mean diameter of about 5 μm and a purity of 99.99%. Figure 2b shows a scanning electron microscope image of the tungsten powder.

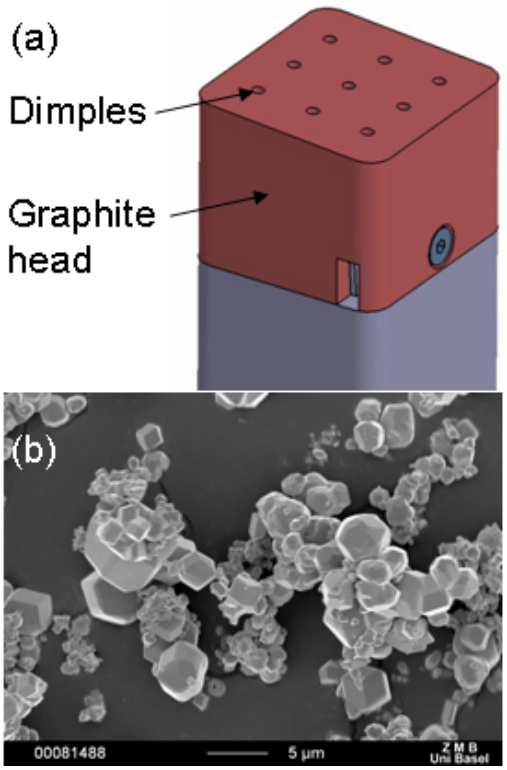

Figure 2. (a) Schematic drawing of the DSF graphite head used for the dust exposure experiments. The powder is placed inside the 9 dimples made on plasma-exposed surface of the DSF head. (b) SEM picture of the tungsten dust.

2.3. Stereoscopic imaging of the dust motion

The relative open vessel design of MAST as well as the large vacuum to plasma volume ratio makes MAST exceptionally suited for optical diagnostics. Two fast infrared cameras are used to image the dust motion in the divertor plasma: a Santa Barbara Focal Plane system (SBFB 125, 320x256 pixels) which measures IR radiation in the wavelength range of 3 to 5 μm (MWIR) and a Thermosensorik CMT256 L HS camera with a 256x256 pixel focal plane array detector sensitive in the 7.6-8.9μm wavelength range (LWIR). More details about the MAST infrared system can be found in [14]. Both cameras were synchronized in time (using the same clock signal) and were set up for a framerate of 315 hz and full frame data acquisition. The cameras are installed on the same port on the lower divertor of MAST and give a tangential view of the outer divertor (figure 3) and of the DSF.

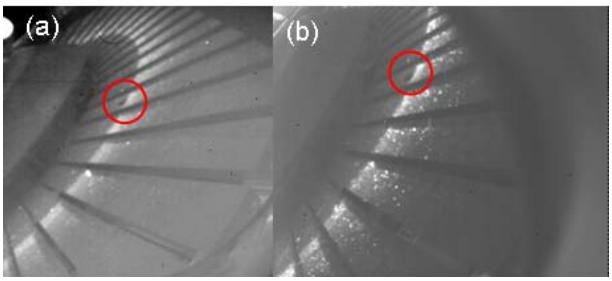

Figure 3. Tangential view from the lower outer divertor of MAST as seen by the (a) LWIR and (b) MWIR cameras. The location of the DSF probe head is indicated on each view by the red circle.

The alignment of the cameras with respect to the MAST coordinate system is determined using the LEON code [16]. The model of MAST within LEON is based on coordinates from the original CAD drawings of the tokamak and its components. A 3D model of the section of the tokamak being observed is overlaid on the 2D camera picture. Reference points are chosen on both the 3D model and the 2D picture, and a fitting routine adjusts the virtual camera orientation and position. The sight line corresponding to each pixel in the MAST coordinate system can then be reconstructed.

The two-dimensional tracks of the followed particles are identified for both cameras. The 3D coordinates of the particle are assumed to be those of the the middle point of the shortest line between two sight lines belonging to both views. In theory, both sight lines should actually cross but in practice they don't because of the accuracy in the camera alignment. The accuracy of the 3D reconstruction is about 3 cm and has been determined from the observation of particles bouncing back from plasma-exposed surfaces whose coordinates are known.

3. Results and discussion

3.1. Dust motion during disruptions

Large amounts of dust particles are usually observed following a disruption. Figure 4 shows 2 infrared images from the MWIR camera looking at the upper divertor region during an upwards moving Vertical Displacement Event (VDE). The exposure time of the camera was quite long (1 ms) so that the particles appear as straight lines. The particle velocity is estimated from the length of these tracks and the knowledge of the camera spatial resolution. Velocities in the range of 80-350 m.s^{-1} have been observed while the mean velocity is about 160 m.s^{-1}, which is slightly higher than that reported in [9] (100 m.s^{-1}). Interestingly, the particles seem to be released isotropically from the surface which would be consistent with release due to brittle destruction. This effect occurs for brittle materials submitted to thermal stresses and is usually accompanied by crack formation and propagation, and particle release. The range of particle velocity observed during disruptions in MAST is actually consistent with observations from Hirai et al during transient heat load testing of carbon based materials [17].

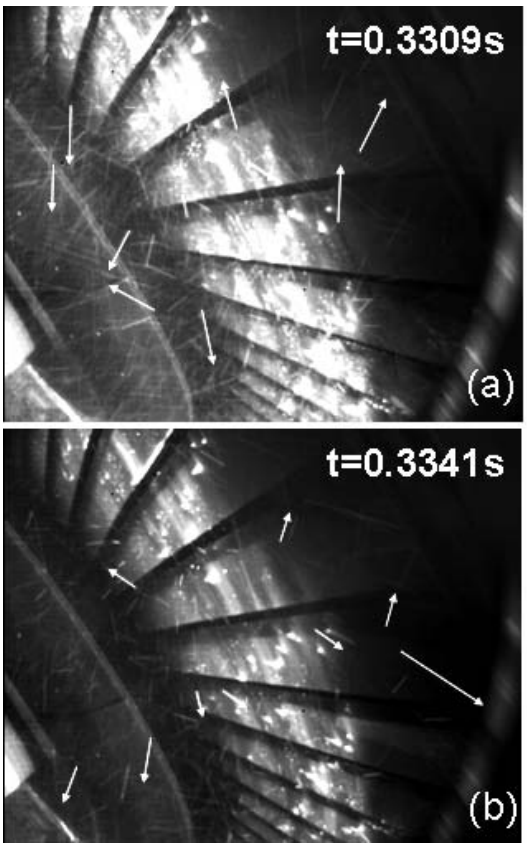

Figure 4. Infrared images of dust particles motion from the upper divertor following a VDE. Pictures are taken (a) 6 ms and (b) 9 ms after the beginning of the disruption. The white arrows are indications of the direction of the motion of some particles.

3.2. Impact of dust particles on the plasma performance

Carbon and tungsten dust particles were injected in the divertor plasma during similar ohmic L-mode discharges. The strike-point position is swept during the discharge and remains at the DSF location for about 40 ms (figure 5d). Figure 5 shows a comparison of the main plasma parameters during a reference discharge (no dust injection), and discharges with carbon and tungsten dust injection. The traces correspond to the first discharge after the introduction of the DSF. Most of the dust is taken away during that first discharge. In the case of carbon dust release from the DSF head is observed during the following 4-5 discharges, on the contrary all the tungsten dust (similar quantity) seems to be mobilized during the first discharge. The most striking feature of these experiments is that the discharge duration seems to vary inversely with the dust atomic number. In the tungsten case, the discharge disrupts about 150 ms earlier than the reference discharge while the disruption occurs 80 ms early in the carbon case.

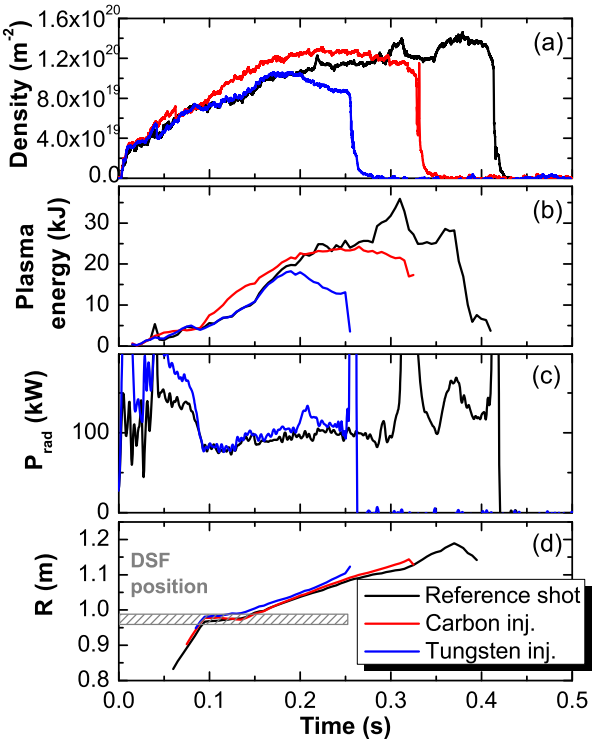

Figure 5. Evolution of the main plasma parameters during the carbon and tungsten dust injection experiments: (a) line-averaged density, (b) plasma stored energy, (c) radiated power as measured by bolometry (the bolometer was not working during the carbon dust experiment) and (d) evolution of the strike-point position (the position of the DSF probe head is indicated by the grey shaded area).

The bolometers were not available during the carbon dust injection, so only the

data concerning tungsten will be described. A significant rise of the radiated power occurs around 100 ms after the strike-point reaches the DSF position figure (5c). This is immediately followed by a strong decrease of the plasma stored energy and density(figure 5b), the plasma termination occurs around 60 ms later. The discharge density and stored energy in the carbon case are slightly different from those of the reference discharge, but since the divergence between both appears slightly before the outer strike-point reaches the DSF surface it is not clear whether this is a dust related effect or whether the differences can be explained by different wall conditions of the machine between the reference discharge and the dust injection experiment. In any case, those experiments demonstrate that the presence of dust in the plasma-wetted area of the divertor could have a significant impact on the plasma performance, especially in the case of high-Z materials like tungsten.

3.3. Dust motion in the divertor plasma

Figure 6 shows the trajectories, in (r, z, ϕ) coordinates, of some representative particles followed during the dust injection experiments. Both carbon and tungsten particles exhibit similar motion. The particles move toroidally in the direction of the toroidal field, they move radially outwards and vertically upwards, i.e. towards the main plasma. It appears that all the particles move in the same toroidal direction. Although, the toroidal motion direction in NSTX was dependent on whether the particles were located outboard or inboard of the outer strike-point [18], this is not observed in the present case. It appears that tungsten particles are in general more prone to vertical motion towards the main plasma than the carbon particles, this can be seen in the projections of the trajectories on the (z,ϕ) plane shown in figure 6. This might explain the very early plasma terminations during the tungsten dust injection experiment.

It should be pointed out that this vertical motion actually implies that there exists a component of the particle velocity which is perpendicular to the magnetic field (poloidal+toroidal) in the divertor, and thus perpendicular to the plasma flow which is directed towards the divertor surface. It is generally acknowledged that the dominant force acting upon a dust particle in the edge plasma is the drag force from the plasma flow [19, 20]. To be released from the surface, the dust particles should thus have an initial velocity which is directed perpendicular to the divertor magnetic field. The issue of dust mobilization from a plasma-exposed surface is usually not treated in the existing dust transport codes like DUSTT [19] or DTOKS [21], instead an initial velocity and direction is assumed for the particles. In order to be released from the wall, it is necessary to overcome the forces maintaining the particles on the surface like gravity (in the present case of a horizontal surface) and the adhesive Van der Walls force [22]. The release of the particles will then depend on the orientation of the magnetic field towards the surface and the wall potential [23]. The cited studies, however, do not analyze the motion of the released particles, although it is not unreasonable to assume that without a upwards directed initial velocity the particles would actually not be able to leave the

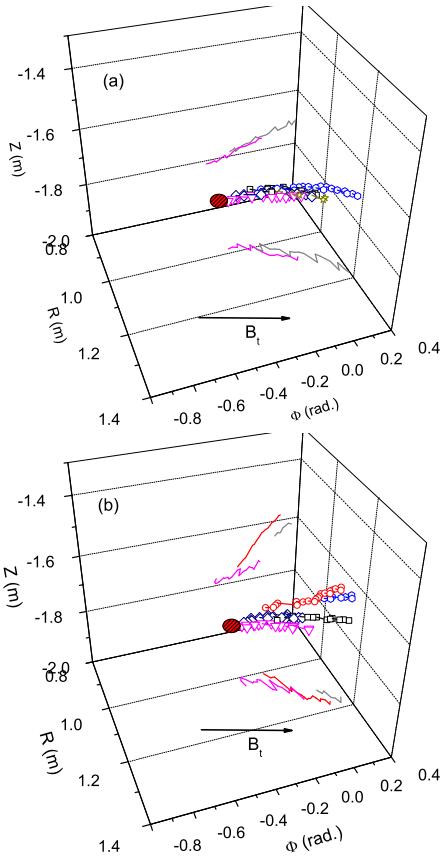

Figure 6. Particle trajectories during the dust injection experiments for (a) carbon and (b) tungsten particles. The position of the DSF is marked with a dashed circle. Projections of some trajectories in the (z,ϕ) and (R,ϕ) planes are also shown.

surface.

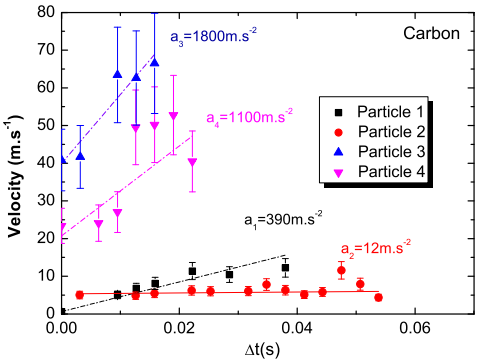

Figure 7. Time evolution of the particle velocity of carbon dust particles.

The particle velocities are determined from the 3D tracks by calculating the motion distance between 2 subsequent frames. Figure 7 shows the time evolution of the velocity

of different carbon particles during the discharge. The observed velocities are in the range 1-100 m.s^{-1}, but a strong scatter exists for the different individual particles. The acceleration the particle experience in the plasma lies in the range 5-2000 m.s^{-2} and appears to be correlated with the apparent particle size- the smaller the particle the larger the acceleration. The precise particle size cannot be determined from the infrared camera pictures but a trend can be drawn. The carbon particles size distribution [13] has a certain spread (between 1 and 20 μm) and in addition it is not unreasonable to suspect that agglomeration of some particles could have occurred when the dust was loaded onto the DSF head (through compaction for example).

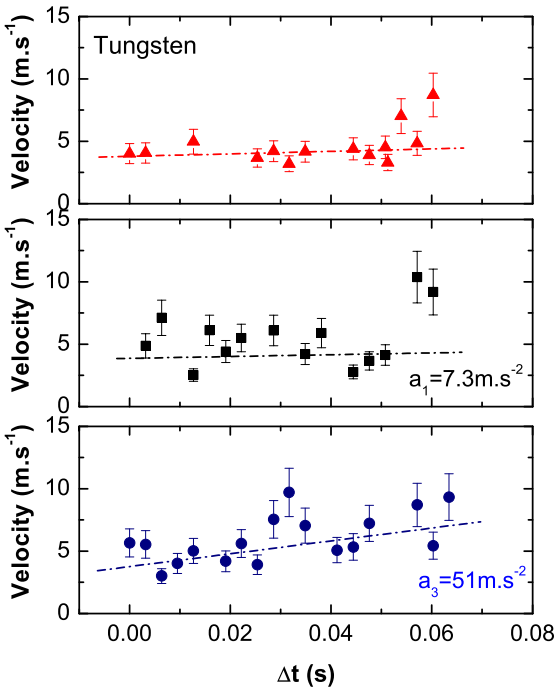

Figure 8. Time evolution of the particle velocity of carbon dust particles.

The behaviour of the tungsten particles is very different, with a much narrower velocity distribution. Figure 8 shows an example of the temporal evolution of the velocity of 3 particles, they are plotted on three different graphs for ease of reading. The observed velocities are in the range 5-30 m.s^{-1} which is much lower than the observed velocities of the carbon particles. Similarly the acceleration experienced by the particles is in the range 0-100 m.s^{-2}. The general trend is that the particles are weakly accelerated by the plasma, whereas some particles appear to experience almost no acceleration and exhibit a constant velocity for the 80-90 ms during which they are visible by the infrared cameras.

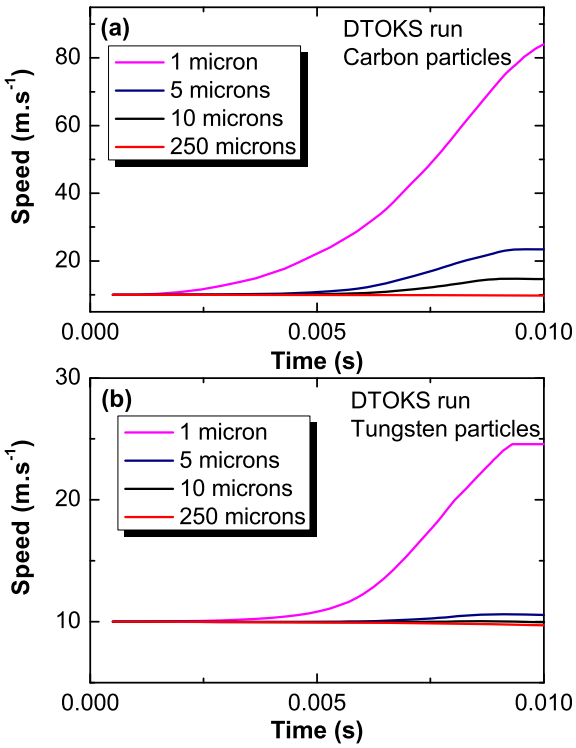

Figure 9. Results of a DTOKS simulation to study the influence of the particle size on the time evolution of the particles velocity. Carbon (a) and tungsten(b) particles are injected with an initial vertical velocity of 10 m.s^{-1}.

The DTOKS code has been used to study the influence of the dust size and composition on the particle velocity. The particles are injected from the DSF location with a vertical velocity of 10 m.s^{-1}. Spherical particles are considered. Results are shown in figure 9. In both cases, the smaller the particles the larger the experienced acceleration. This is in good agreement with the camera observations. For carbon particles, the acceleration experienced by a 5 microns particle is around 300 m.s^{-2} while it is about 12000 m.s^{-2} for a 1 micron particle. The former is in good agreement with what is experimentally observed for particle 1 in figure 7, while the latter is much larger than the experimentally observed values. This might indicate that the observed particles are all larger than 1 μm. In addition, the behavior of particle 2 in figure 7 would be consistent with the code prediction for a large size particle. For tungsten, the experimentally observed behaviour (figure 8) is consistent with DTOKS predictions for particle size in the range 5-10 μm which actually constitute the core of the particle size distribution. A detailed experiment/code comparison will be the subject of a separate

paper but those initial results shed some light on the experimental observations and confirm the different behaviour of carbon and tungsten particles.

4. Conclusions

The release of dust particles from the upper divertor of MAST during disruptions has been studied using a fast infrared camera. Large amounts of dust particles are generated during VDEs, with velocities in the range 80-350 $m.s^{-1}$. The particle release appears to be isotropic which would be consistent with release due to brittle destruction of the graphite tile surface or co-deposited layers on the tile surface.

The motion of tungsten and carbon dust particles, with known size distributions, in the divertor plasma has been studied by stereoscopic imaging. The newly installed divertor probe has been used to expose particles in the outer divertor of MAST and their motion was followed with 2 fast infrared cameras. The mobilization of dust by the plasma is found to significantly affect the plasma performances, with early disruptions. The effect is more pronounced for tungsten particles. A correlation between the carbon particle size and acceleration by the plasma is observed. Tungsten particles are found to move with lower velocities and experience lower acceleration and are found to be more prone to vertical motion. Initial modelling of the experiments using the DTOKS code has been done. The observed velocity range and acceleration are well reproduced by the code.

Those results show that dust generated during a disruption and settling on plasma exposed surfaces might represent a serious concern for the performances of the following discharges especially in the case of high-Z materials like tungsten.

5. Acknowledgments

CCFE and Imperial College authors were funded by the UK EPSRC. This work, supported by the European Communities under the contract of Association between EURATOM and CCFE, was carried out within the framework of the EFDA Task Force on Plasma Wall Interactions. The views and opinions expressed herein do not necessarily reflect those of the European Commission.

References

[1] Winter J. 1998 *Plasma Phys. Contr. Fusion* 40 1201
[2] Narihara K. *et al* 1997 *Nucl. Fusion* 37 1177
[3] Saito K. *et al* 2007 *J. Nucl. Mater.* 363-365 1323
[4] Pegourie B. *et al* 2009 *J. Nucl. Mater.* 390-391 550
[5] Rosanvallon S. *et al* 2009 *J. Nucl. Mater.* 390-391 57
[6] Grisolia C. *et al* 2009 *J. Nucl. Mater.* 390-391 53
[7] Federici G. *et al* 2001 *Nucl. Fusion* 227
[8] Winter J. *Plasma Phys. Contr. Fusion* 46 B583
[9] Yu J.H. *et al* 2009 *J. Nucl. Mater.* 390-391 216

[10] Garkusha I.E. *et al* 2009 *Phys. Scr.* T138 014054
[11] Wong C.P.C *et al* 1998 *J. Nucl. Mater.* 258-263 433
[12] Darke A.C. *et al* 2005 *Fusion Eng. Des.* 75-79 285
[13] Rudakov D.L. *et al* 2007 *J. Nucl. Mater.* 363-365 227
[14] De Temmerman G. *et al* 2010 *Plasma Phys. Contr. Fusion* submitted
[15] Boeglin W.U. *et al* 2008 *Rev. Sci. Instrum.* 79 10F334
[16] Lott F. 2007 *PhD thesis, Imperial College London*
[17] Hirai T. *et al* 2004 *Phys. Scr.* T111 163
[18] Roquemore A.L. *et al* 2007 *J. Nucl. Mater.* 363-365 222
[19] Krasheninnikov S.I. *et al* 2004 *Phys. Plasmas* 11 3141
[20] Krasheninnikov S.I. *et al* 2008 *Plasma Phys. Contr. Fusion* 50 124054
[21] Martin J.D. *et al* 2008 *EPL* 83 65001
[22] Flanagan T.M. and Goree J. 2006 *Phys. Plasmas* 13 123504
[23] Tomita Y. *et al* 2009 *J. Nucl. Mater.* 390-391 164